Letter

Phase separation in a mixture of proliferating and motile active matter

Lukas Hupe,[1] Joanna M. Materska,[2] David Zwicker,[1] Ramin Golestanian,[1,3,*] Bartlomiej Waclaw,[2,4,†] and Philip Bittihn[1,‡]

[1]*Max Planck Institute for Dynamics and Self-Organization, Göttingen, Germany*
[2]*Dioscuri Centre for Physics and Chemistry of Bacteria, Institute of Physical Chemistry, Warsaw, Poland*
[3]*Rudolf Peierls Centre for Theoretical Physics, University of Oxford, Oxford OX1 3PU, United Kingdom*
[4]*School of Physics and Astronomy, The University of Edinburgh, Edinburgh EH9 3FD, United Kingdom*

(Received 11 June 2025; accepted 9 March 2026; published 13 April 2026)

Proliferation and motility are ubiquitous drivers of activity in biological systems. Here, we study a dense binary mixture of motile and proliferating particles with exclusively repulsive interactions, where homeostasis in the proliferating subpopulation is maintained by pressure-induced removal. Using numerical simulations, we show that phase separation emerges naturally in this system at high density and weak enough self-propulsion. We map the full two-component system to an effective single-component active Brownian particle model that recapitulates this behavior. This allows us to identify the emergent effects of the proliferating matrix on motile particles that interact to produce phase separation: enhanced diffusion, renormalized self-propulsion, reduced persistence, and an effective attraction between motile particles. Our results establish a specific type of phase transition based on these emergent effects and pave a way to reinterpret the physics of dense cellular populations, such as bacterial colonies or tumors, as systems of mixed active matter.

DOI: 10.1103/9pns-h5ll

Introduction. Out-of-equilibrium, active matter systems made of self-driven entities such as motile bacteria, synthetic colloids, and flocking animals exhibit a rich array of collective phenomena, including motility-induced phase separation (MIPS), flocking transitions, and defect formation. While significant progress has been made in understanding phase separation within single-component active matter systems [1–9], the interplay between distinct types of active matter remains largely unexplored.

Most theoretical and experimental studies have focused on motile active matter, characterized by self-propelled particles that interact through forces and torques, leading to phenomena ranging from emergent swarming behavior to clustering dynamics [10–14]. Systems featuring growing active matter, where particle populations expand through division and growth [15], have received comparatively less attention. Notable works in this domain include studies on growing bacterial colonies, as well as investigations into the mechanical feedback and pattern formation in tissues and biofilms [16–23]. These studies underscore the unique physical constraints and emergent behaviors arising from growth-induced stresses and homeostatic regulation.

However, many naturally occurring systems feature both motile and growing active matter. For example, biofilms often consist of growing bacterial populations interspersed with motile bacteria that swim through the porous matrix [24,25]. Similarly, cancerous tissues exhibit a dynamic interplay between proliferating cells and motile cells undergoing epithelial-to-mesenchymal transition (EMT) [26]. This highlights the need for a systematic understanding of how growth and motility interact and shape collective behaviors. Previous studies have begun to address related questions, such as the clustering of passive particles in an active bath [27–29], segregation of rods with different levels of activity [30], multiple species interacting nonreciprocally [31–33], and shape-dependent segregation in growing colonies [34]. Moreover, recent work on motile and nonmotile or slowly motile cells further emphasizes the relevance of mixed active matter systems [35,36].

From a theoretical perspective, it is intriguing that the properties underlying known transitions in systems of only motile particles could be fundamentally altered by the presence of a growing phase: For example, in flocking, the ratio of rotational diffusion to velocity governs the transition to collective motion in the presence of aligning interactions [10]. For MIPS, density-dependent self-propulsion leads to phase separation [5]. The addition of growing particles introduces new timescales and interactions that could modify these properties, leading to new effective interactions between motile particles, potentially introducing new kinds of collective behavior.

In this work, we propose a simple, idealized model that combines motile and growing active matter to investigate how

*Contact author: ramin.golestanian@ds.mpg.de
†Contact author: bwaclaw@ed.ac.uk
‡Contact author: philip.bittihn@ds.mpg.de

Published by the American Physical Society under the terms of the Creative Commons Attribution 4.0 International license. Further distribution of this work must maintain attribution to the author(s) and the published article's title, journal citation, and DOI. Open access publication funded by Max Planck Society.

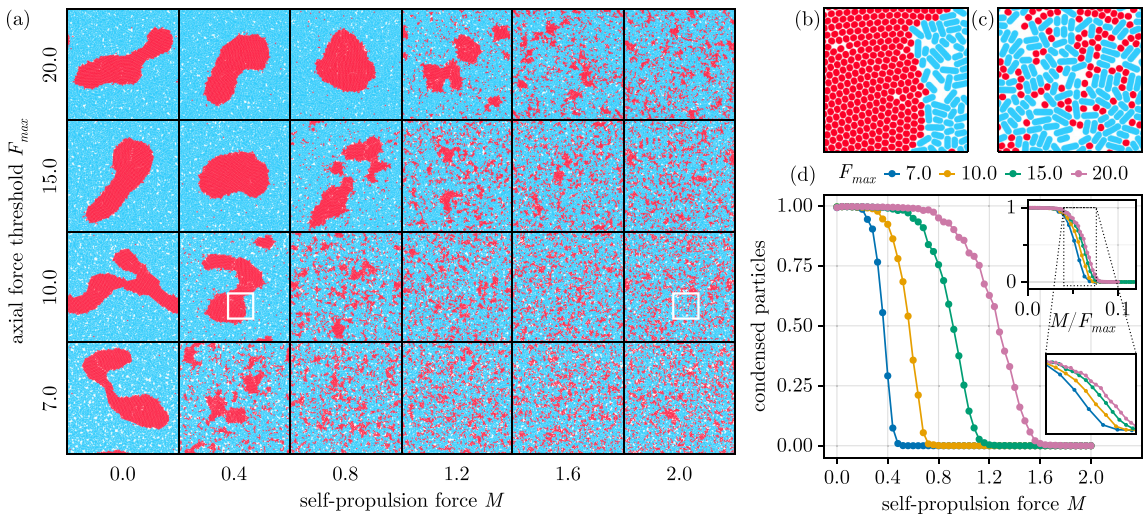


FIG. 1. (a) Snapshots of mixtures of motile (red) and growing (blue) particles at $t = 2 \times 10^4$, for different combinations of self-propulsion force M and axial force threshold $F_{\max}$, showing a transition from a phase-separated regime (top left) to a mixed regime (bottom right). White squares represent regions shown in panels (b) and (c). (b) An enlarged view of a phase boundary, for $M = 0.4$ and $F_{\max} = 10.0$. (c) An enlarged view of the mixed phase, for $M = 2.0$ and $F_{\max} = 10.0$. (d) Fraction of motile particles in clusters of more than 300 particles as a function of self-propulsion force M, for different axial force thresholds $F_{\max}$. Inset: The same data with the self-propulsion force rescaled by $F_{\max}$.

these two types of activity interact and coevolve. We show that, when the activity of the growing phase is sufficiently strong compared to the activity of the motile phase, the motile phase undergoes a condensation transition that has not been observed in single-component active matter models. Our findings shed light on the rich interplay between motility and growth, and demonstrate how important it is to consider these interactions in real-world systems such as biofilms, tissues, and other heterogeneous active matter systems.

Model. We extend the particle-based model [37] of two-dimensional spherocylinders interacting through steric repulsion. All particles have the same width, equal to one unit of length. Growing cells elongate linearly in time, each with a slightly different rate, and divide symmetrically into two cells upon reaching a preset maximum length. Nongrowing, motile cells have a constant, slightly anisotropic shape with an aspect ratio of 1.1 to enable them to rotate in response to external forces. They self-propel with a force of magnitude M along their axis. Cell dynamics follow overdamped equations of motion, with individual center of mass positions $\boldsymbol{r}_{\mathrm{cm}}$ and orientations ϕ evolving as

$$\partial_t \boldsymbol{r}_{\mathrm{cm}} = \underline{\boldsymbol{\mu}}_{\mathrm{t}} \cdot [\boldsymbol{F}_{\mathrm{st}} + M\,\hat{\boldsymbol{e}}(\phi)], \quad \partial_t \phi = \mu_{\mathrm{rot}}\, T_{\mathrm{st}}, \tag{1}$$

where $\hat{\boldsymbol{e}}(\phi)$ is the unit vector along the cell axis, $\boldsymbol{F}_{\mathrm{st}}$ and T_{st} are translational forces and torques due to steric interactions, and M is the self-propulsion force (only $\neq 0$ for motile cells). Details on the computation of steric forces and the choice of mobilities $\underline{\boldsymbol{\mu}}_{\mathrm{t}}$ and μ_{rot} can be found in Supplemental Material [38] and Ref. [37].

Total cell density is kept approximately constant by removing growing cells when their axial compression force, computed from the antisymmetric component of the steric forces acting on both nodes [see Fig. S1(a) in Supplemental Material [38]], exceeds a threshold $F_{\max}$. Force units are arbitrary, but cell overlaps necessary to reach the thresholds $F_{\max}$ used in this study are given in Supplemental Material [38]. For growing cells, the distribution of the elongation rates is such that the average doubling time is one time unit. The system is simulated in a square box of size 80×80 with periodic boundaries, for 2×10^4 generations. For further details, see Supplemental Material [38].

Results. Figure 1(a) illustrates the final state of these simulations for different values of the self-propulsion M and critical compression $F_{\max}$. We observe that for high compression $F_{\max}$ and low motility M, motile cells condense into a single large, densely packed cluster [Fig. 1(b)]. Increasing motility M makes the cluster decrease in size and break up, until only a mixed motile-growing phase remains at high M [Fig. 1(c)]. Measuring the fraction of condensed motile cells quantitatively confirms a transition from full condensation to a mixed state with onset at nonzero M [Fig. 1(d)]. Since $F_{\max}$ modulates the typical forces exerted by growing particles at homeostasis, this indicates that the behavior of motile particles is also modified. Interestingly, when rescaling the x axis to $M/F_{\max}$, the curves almost collapse, although a small shift of the transition point with increasing $M/F_{\max}$ remains [Fig. 1(d), insets]. This approximate collapse suggests that the transition to phase separation is primarily governed by a balance of motility with the forces exerted by the surrounding growing medium.

Since all explicit interactions in our system rely on contact-based forces, any additional interactions between nongrowing cells that could potentially lead to this phase separation must be mediated by the growing medium. To characterize these potential changes induced by nongrowing particles, we therefore start with the simplest case: a single nongrowing "tracer" immersed in the growing medium, which acts as a bath.

Since the removal of particles is triggered by mechanical stress, interactions between the bath and tracer could affect the local turnover rate. We thus define the local turnover imbalance $\lambda = \kappa_{\mathrm{add}} - \kappa_{\mathrm{div}} - \kappa_{\mathrm{rem}}$ per unit area, where κ_{add}, κ_{div}, and κ_{rem} are the (position-dependent) rates at which daughter

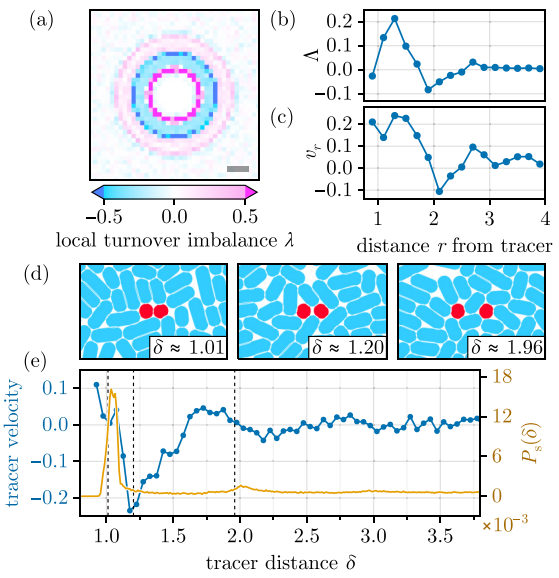


FIG. 2. (a) Local turnover imbalance λ around a single tracer particle. Scale bar shows a distance of one cell width. (b) Integrated turnover imbalance Λ as a function of distance from tracer center. (c) Radial bath particle center position velocity v_r as a function of distance from tracer center. (d) Snapshots of test simulations of two tracers in an active bath for different tracer distances δ. (e) Relative tracer drift velocity as a function tracer distance δ (blue, left-hand axis), and steady-state distribution of pair distances $P_s(\delta)$ (orange, right-hand axis).

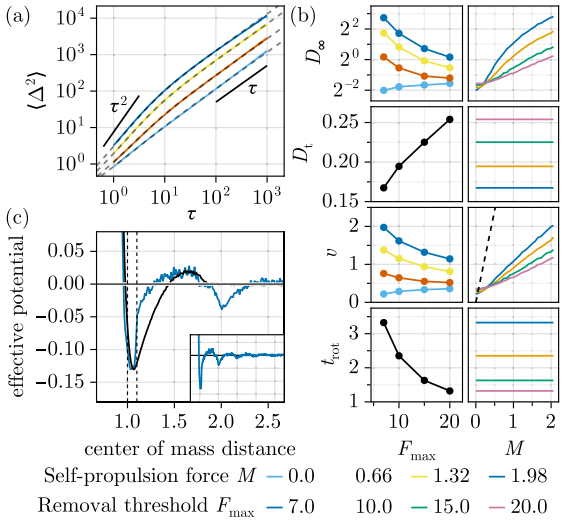


FIG. 3. (a) Mean squared displacement $\langle\Delta^2\rangle$ of a single self-propelled tracer in a growing bath, computed over 10^5 generations, for different self-propulsion forces M and a fixed $F_{max} = 10.0$. Dashed lines represent the best-fit active-particle MSD [Eq. (2)]. (b) Best-fit parameters [Eq. (2)]: effective long-term diffusion coefficient D_∞, translational diffusion D_t, self-propulsion velocity v, and persistence time t_{rot}. Fitting was constrained so that D_t and t_{rot} could not vary with M. Dashed black line in the v plot represents the "bare" velocity of motile particles. (c) The effective interaction potential, obtained for two passive tracer particles in a growing bath with $F_{max} = 10.0$ (blue), and for ABPs using the simple linear adhesion force model (black) with parameters matched to the two-component model. Inset: The potential for longer interparticle distances up to 5.5.

cells are added after division, mother cells are removed for division, and cells are removed due to the compression-induced removal mechanism, respectively [39]. Figure 2(a) shows a narrow ring of positive turnover imbalance corresponding to surplus proliferation, surrounded by a wider band of surplus deaths, and finally another band of surplus replications. These local turnover imbalances are due to divisions in the layer of bath particles immediately in contact with the tracer, as the center positions of dividing and newly born particles must fall within certain distances from the tracer due to their characteristic sizes (small newly born particles versus large dividing particles).

The cumulative radial turnover imbalance $\Lambda(r) = \frac{1}{\pi r^2}\int_0^r r'\,\mathrm{d}r'\int_0^{2\pi}\lambda(r',\phi)\,\mathrm{d}\phi$ shows that outside the ring structure (beyond approximately three cell widths from the tracer center), turnover remains balanced [Fig. 2(b)]. Therefore, turnover imbalances merely correspond to local redistributions of particle positions. This is confirmed by the radial velocity distribution of bath particles relative to the tracer, which shows movement from regions of surplus additions to surplus removals [Fig. 2(c)]. Single nongrowing particles are therefore able to exert a short-range influence on the bath of growing cells.

To see whether this effect is bidirectional, i.e., perturbations of the growing bath affect other nongrowing particles, we introduce a second passive tracer particle into our test simulations. Measuring the average relative drift velocity of the tracers as a function of tracer center distance δ [see snapshots in Fig. 2(d)], we observe no significant effect beyond $\delta \approx 2$ [Fig. 2(e)], but a region of negative relative drift for tracer distances between 1 and 1.6.

These results reinforce our conjecture that the growing bath introduces effective interactions between individual nongrowing particles. In addition, the growing bath particles can also be expected to influence *single* nongrowing particles: In absence of a growing matrix, a single motile particle would self-propel ballistically with constant speed (determined by M and the particle mobility) and infinite persistence time. Steric interactions with a growing matrix introduce quasirandom translational forces and torques, giving rise to diffusive behavior, and reducing the effective self-propulsion speed.

To find out whether these effects of the growing bath are sufficient to enable phase separation and how they conspire quantitatively to do so, we now examine a model with only motile particles. For this, we hypothesize that the interactions with the growing phase can be modeled by random thermal excitations that, together with self-propulsion, yield behavior akin to active Brownian particles (ABPs) for the motile particles. Further below, we will include a deterministic short-range force to capture the effective interaction between pairs of motile particles.

To parametrize this single-component model, we first simulate the full two-component model, but with only a single motile particle immersed in the growing bath. We then obtain this particle's mean squared displacement (MSD) $\langle\Delta^2\rangle(\tau)$ for different M and F_{max}. Figure 3(a) shows diffusive motion

on long timescales and ballistic motion at shorter timescales for nonzero motility M. As hypothesized, this is consistent with behavior of an ABP with translational diffusion D_t, self-propulsion with velocity v, and persistence time t_rot. Its MSD follows [40,41]

$$\Delta^2(\tau) = (4D_\mathrm{t} + 2v^2 t_\mathrm{rot})\tau + 2v^2 t_\mathrm{rot}^2 (e^{-\tau/t_\mathrm{rot}} - 1), \quad (2)$$

with a long-term effective diffusion coefficient of $D_\infty = D_\mathrm{t} + v^2\, t_\mathrm{rot}/2$. Fitting this function to the mean squared displacement of such single motile particles immersed in the growing bath [Fig. 3(a)] allows us to obtain estimates for the effective ABP parameters as functions of F_max and M. To keep the model minimal, we assume that D_t and t_rot are purely determined by interactions with the bath and thus do not vary with M. Figure 3(a) shows that this model fits the measured MSD very well.

The inferred parameters are shown in Fig. 3(b). We observe that the translational diffusion coefficient increases with F_max, consistent with higher death-induced activity at higher compression thresholds. For most values of M (except very small ones), the inferred velocity v is lower than the bare self-propulsion velocity [dashed line in the M–v plot, Fig. 3(b)] due to bath-induced friction. Consistent with this, both the inferred self-propulsion velocity v and persistence time t_rot decrease with increasing F_max, corresponding to an increased inhibition of persistent self-propulsion at higher densities. This effect also dominates the effective long-term diffusion coefficient D_∞, which decreases substantially with higher F_max if M is not too small.

Interestingly, for very small M, v does not vanish and the dependence on F_max reverses, so that v increases with density, implying that bath motion is not purely diffusive at short timescales. This is consistent with prior studies on similar models [42,43], which found evidence of ballistic motion at short times and less persistent motion at higher densities.

An ABP model with these parameters can therefore reproduce the single-particle behavior of the original two-component simulations. To include the short-range attraction as observed in Fig. 2(e) in our effective description, we now introduce an effective adhesion force between two ABPs. For this, we neglect the small anisotropy of motile particles and model the adhesion with an isotropic interaction potential V depending only on the distance δ between particle centers. According to the Fokker-Planck equation of a particle moving in this potential with mobility μ and diffusion coefficient D_t, we can define the effective potential as

$$V(\delta) = -\frac{2D_\mathrm{t}}{\mu} \ln P_\mathrm{s}(\delta), \quad (3)$$

where $P_\mathrm{s}(\delta)$ is the steady-state distribution of interparticle distances δ measured in simulations of pairs of tracer particles (averaged over the polar angle according to the assumed rotational symmetry) as also shown in Fig. 2(e). Figure 3(c) shows the effective potential computed in this way for $F_\mathrm{max} = 10$. We observe strong attraction near the tracer, followed by a repeating pattern of attraction and repulsion, with a period of approximately one cell width and quickly decaying amplitude, which is likely caused by the finite size of the bath particles. However, for simplicity, we only model the initial potential well and barrier with a simple linear force law and corresponding potential,

$$V(r) = -\Delta V \left(\frac{r}{r_b} - 1\right)^2 + V_b, \quad (4)$$

for $0 < r \leqslant r_2\,(1 + \sqrt{V_b/\Delta V})$ with the potential well depth ΔV and barrier height V_b fitted to $V(r)$ from the two-component simulation (see Supplemental Material [38] for details). Figure 3(c) shows excellent agreement between the effective potentials determined via Eq. (4) in two-component simulations and ABP simulations.

The complete single-component model now consists of the ABP core component incorporating translational diffusion with coefficient D_t, self-propulsion velocity v, and persistence time t_rot, the linear adhesion model, and steric interactions and equations of motion of the existing rod model. The equations of motion for a single particle in this effective description are

$$\partial_t \boldsymbol{r}_\mathrm{cm} = v\,\hat{\boldsymbol{e}}(\phi) + \sqrt{2D_t}\boldsymbol{\xi}_t(t) + \underline{\boldsymbol{\mu}}_\mathrm{t} \cdot (\boldsymbol{F}_\mathrm{st} + \boldsymbol{F}_\mathrm{adh}), \quad (5a)$$

$$\partial_t \phi = \sqrt{2/t_\mathrm{rot}}\,\xi_\mathrm{rot}(t) + \mu_\mathrm{rot}(T_\mathrm{st} + T_\mathrm{adh}), \quad (5b)$$

where $\boldsymbol{\xi}_\mathrm{t}$ and ξ_rot are Gaussian noise terms with unit variance, $\boldsymbol{F}_\mathrm{adh}$ and T_adh are forces and torques due to the effective adhesion potential, and $\boldsymbol{r}_\mathrm{cm}$, ϕ, $\hat{\boldsymbol{e}}(\phi)$, $\boldsymbol{F}_\mathrm{st}$, and T_st are defined as in Eq. (1). This model thus replaces the implicit stochasticity and attraction between motile particles in the original system (arising from interactions with the proliferating phase) by explicit noise terms in analogy to classical ABPs and the explicit adhesion potential, respectively.

Figure 4(a) shows snapshots of simulations using inferred parameters corresponding to different M and F_max. We see a clear transition from the condensed to the mixed state, showing that the single-component model qualitatively captures the behavior of the full model from Fig. 1(a). The fact that the particles do not condense into a single cluster within the simulation time is likely due to slow condensation dynamics, because single clusters do not evaporate once formed (Fig. S3 in Supplemental Material [38]). The fraction of condensed particles [Fig. 4(b)] confirms the presence of the phase transition, albeit at slightly higher values of M than in the two-component model.

Discussion. We have demonstrated that a heterogeneous active mixture of growing and motile particles spontaneously separates into two phases for a range of model parameters. The two types of activity, growth and motility, oppose each other: Growing particles exert an effective pressure that tries to condense motile particles, whereas motile particles try to overcome this dynamic confinement. The onset of condensation is governed by a balance between self-propulsion and the typical forces exerted by the surrounding growing bath. Note that this is in some sense the opposite of MIPS, where higher self-propulsion velocities enable condensation, whereas here self-propulsion *overcomes* an effective attraction that is always present. We also show that a model with only one species of active Brownian particles and an effective attraction captures the effects of the growing phase on motile particles and qualitatively reproduces the condensation phenomenon. It will be important to uncover the mechanism giving rise to this attraction. Among other scenarios, an intriguing possibility is to interpret it as a nonequilibrium Casimir-like force [44], given that all interactions are mediated by ran-

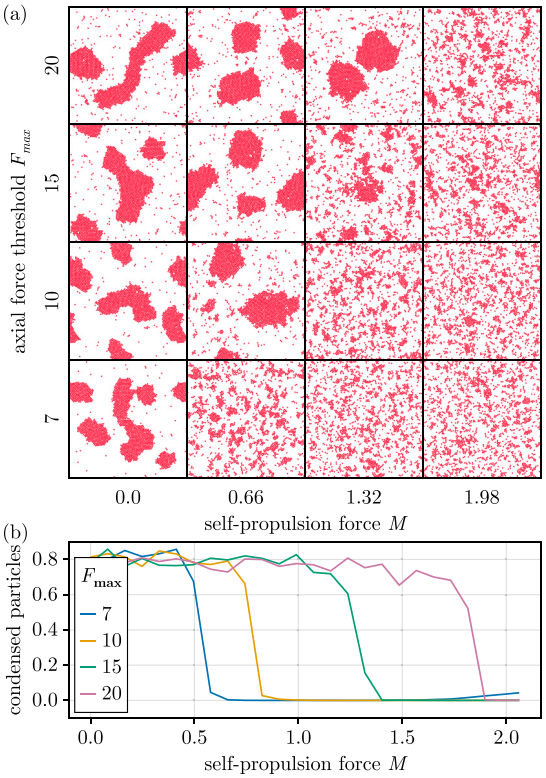


FIG. 4. (a) Snapshots of simulations of the single-component model after 2×10^4 time units, for parameters corresponding to different combinations of self-propulsion force M and axial force threshold $F_{\max}$, showing a transition from a fully phase-separated regime in the top left to a mixed regime in the bottom right. (b) Fraction of particles within clusters of at least 300 particles for parameters corresponding to different self-propulsion forces and removal thresholds.

dom mechanical forces originating from the growing medium. Such analogies have been drawn in other active matter systems with steric interactions, e.g., Ref. [45], where particle depletion due to geometric effects creates effective attractions.

We also observe quantitative differences between the full and the single-component ABP model, most prominently the speed of coarsening after the first clusters have formed, as well as differences in the critical self-propulsion force. One reason could be that our ABP model only encodes pairwise interactions and thermal noise whose magnitudes are independent of the particles' environment. Even in simpler systems, two-body descriptions can be insufficient to fully characterize phase separation (as seen for MIPS of active Brownian particles [46]). Here, the basic assumptions of our effective model neglect many potential many-particle effects: In the full two-component simulations, larger clusters of motile cells might perturb the growing bath more strongly due to their reduced mobility. Indeed, larger nongrowing particles mimicking large clusters cause much longer-ranged perturbations of the growing bath and advection toward them (see Fig. S4 in Supplemental Material [38]) that would enhance accretion of additional particles for existing clusters. In the ABP model, on the other hand, effective adhesion has always the same (short) range. In addition, in the full model, motile particles within a cluster become shielded from the bath, reducing the effective noise they are exposed to. Also, the true force field fluctuates strongly and is non-Brownian at short times. Both features are not accounted for in our approach. Exploring these effects for larger clusters might therefore be worthwhile to delineate the role of higher-order effects and make connections with other nonequilibrium models that exhibit condensation [47,48]. For example, reduced diffusivity within clusters might lead to contributions similar to Bose-Einstein condensation due to diffusivity edge [9,49].

The phase-separated clusters in our simulations exhibit irregular, noncircular shapes. We observe that motile particles within clusters form highly ordered, crystal-like domains [e.g., Fig. 1(b)], which could inhibit shape relaxation through jamming or reduced particle mobility even near cluster edges.

Finally, many assumptions made here could be relaxed or altered, potentially leading to additional phenomena or substantially changed behavior. For example, we focused on low fractions of motile particles. Exploring the opposite limit, which might be more realistic for, e.g., bacterial sludge bioreactors, may reveal distinct segregation patterns or banding phenomena. We also considered nearly circular motile particles; introducing elongation could lead to nematically ordered clusters. Conversely, considering entirely circular motile particles with explicit alignment terms or experiencing inherent rotational diffusion instead of mechanical torques could elucidate the importance of the balance between the different emergent effects due to a common source (interactions with the growing phase). Finally, the homeostatic removal mechanism will depend on biological context and could be generalized to density-dependent death rates or replaced by entirely random removal, potentially altering fluctuation spectra and effective interactions.

Acknowledgments. We acknowledge support from the Max Planck School Matter to Life and the MaxSynBio Consortium, which are jointly funded by the Federal Ministry of Education and Research (BMBF) of Germany and the Max Planck Society. We also acknowledge support through a Saltire Facilitation Network Award by the Royal Society of Edinburgh, through the FOKUS International program of the Ministry for Science and Culture of Lower Saxony and through the MWK-Scotland initiative of the Ministry for Science and Culture of Lower Saxony. B.W. and J.M.M. thank Dioscuri, a programme initiated by the Max Planck Society (MPG), jointly managed with the National Science Centre in Poland (NCN), and mutually funded by the Ministry of Science and Higher Education of the Republic of Poland (MNiSW) and the German Federal Ministry of Education and Research (BMBF), Grant No. UMO-2019/02/H/NZ6/00003.

*Data availability.*Simulations used for this study were built in Julia [50], using the open-source simulation framework InPartS [51,52]. The implementation of the agent-based models is available as part of the InPartSBiome model library, published in Ref. [53]. Example code for simulation and data analysis is available in Ref. [54]. Visualizations were prepared using Makie.jl [55]. The data that support the findings of this article can be reproduced with the provided code [54].

[1] H. H. Wensink, J. Dunkel, S. Heidenreich, K. Drescher, R. E. Goldstein, H. Löwen, and J. M. Yeomans, Meso-scale turbulence in living fluids, Proc. Natl. Acad. Sci. USA **109**, 14308 (2012).

[2] R. Golestanian, Phoretic active matter, in *Active Matter and Nonequilibrium Statistical Physics: Lecture Notes of the Les Houches Summer School, September 2018* (Oxford University Press, Oxford, UK, 2022), Vol. 112, pp. 230–293.

[3] G. Gompper, R. G. Winkler, T. Speck, A. Solon, C. Nardini, F. Peruani, H. Löwen, R. Golestanian, U. B. Kaupp, L. Alvarez, *et al.*, The 2020 motile active matter roadmap, J. Phys.: Condens. Matter **32**, 193001 (2020).

[4] M. C. Marchetti, J. F. Joanny, S. Ramaswamy, T. B. Liverpool, J. Prost, M. Rao, and R. A. Simha, Hydrodynamics of soft active matter, Rev. Mod. Phys. **85**, 1143 (2013).

[5] M. E. Cates and J. Tailleur, Motility-induced phase separation, Annu. Rev. Condens. Matter Phys. **6**, 219 (2015).

[6] A. P. Solon, J. Stenhammar, M. E. Cates, Y. Kafri, and J. Tailleur, Generalized thermodynamics of phase equilibria in scalar active matter, Phys. Rev. E **97**, 020602(R) (2018).

[7] S. Shankar, S. Ramaswamy, M. C. Marchetti, and M. J. Bowick, Defect unbinding in active nematics, Phys. Rev. Lett. **121**, 108002 (2018).

[8] F. Jülicher, S. W. Grill, and G. Salbreux, Hydrodynamic theory of active matter, Rep. Prog. Phys. **81**, 076601 (2018).

[9] R. Golestanian, Bose-Einstein-like condensation in scalar active matter with diffusivity edge, Phys. Rev. E **100**, 010601(R) (2019).

[10] T. Vicsek, A. Czirók, E. Ben-Jacob, I. Cohen, and O. Shochet, Novel type of phase transition in a system of self-driven particles, Phys. Rev. Lett. **75**, 1226 (1995).

[11] G. Grégoire and H. Chaté, Onset of collective and cohesive motion, Phys. Rev. Lett. **92**, 025702 (2004).

[12] J. Toner and Y. Tu, Long-range order in a two-dimensional dynamical XY model: How birds fly together, Phys. Rev. Lett. **75**, 4326 (1995).

[13] I. Theurkauff, C. Cottin-Bizonne, J. Palacci, C. Ybert, and L. Bocquet, Dynamic clustering in active colloidal suspensions with chemical signaling, Phys. Rev. Lett. **108**, 268303 (2012).

[14] I. Buttinoni, J. Bialké, F. Kümmel, H. Löwen, C. Bechinger, and T. Speck, Dynamical clustering and phase separation in suspensions of self-propelled colloidal particles, Phys. Rev. Lett. **110**, 238301 (2013).

[15] O. Hallatschek, S. S. Datta, K. Drescher, J. Dunkel, J. Elgeti, B. Waclaw, and N. S. Wingreen, Proliferating active matter, Nat. Rev. Phys. **5**, 407 (2023).

[16] J. Ranft, M. Basan, J. Elgeti, J.-F. Joanny, J. Prost, and F. Jülicher, Fluidization of tissues by cell division and apoptosis, Proc. Natl. Acad. Sci. USA **107**, 20863 (2010).

[17] F. D. C. Farrell, O. Hallatschek, D. Marenduzzo, and B. Waclaw, Mechanically driven growth of quasi-two-dimensional microbial colonies, Phys. Rev. Lett. **111**, 168101 (2013).

[18] M. A. A. Grant, B. Wacław, R. J. Allen, and P. Cicuta, The role of mechanical forces in the planar-to-bulk transition in growing escherichia coli microcolonies, J. R. Soc. Interface **11**, 20140400 (2014).

[19] D. Dell'Arciprete, M. L. Blow, A. T. Brown, F. D. C. Farrell, J. S. Lintuvuori, A. F. McVey, D. Marenduzzo, and W. C. K. Poon, A growing bacterial colony in two dimensions as an active nematic, Nat. Commun. **9**, 4190 (2018).

[20] Y. I. Yaman, E. Demir, R. Vetter, and A. Kocabas, Emergence of active nematics in chaining bacterial biofilms, Nat. Commun. **10**, 2285 (2019).

[21] Q. Zhang, J. Li, J. Nijjer, H. Lu, M. Kothari, R. Alert, T. Cohen, and J. Yan, Morphogenesis and cell ordering in confined bacterial biofilms, Proc. Natl. Acad. Sci. USA **118**, e2107107118 (2021).

[22] Y. G. Pollack, P. Bittihn, and R. Golestanian, A competitive advantage through fast dead matter elimination in confined cellular aggregates, New J. Phys. **24**, 073003 (2022).

[23] J. Isensee, L. Hupe, R. Golestanian, and P. Bittihn, Stress anisotropy in confined populations of growing rods, J. R. Soc. Interface **19**, 20220512 (2022).

[24] N. Steinberg, A. Keren-Paz, Q. Hou, S. Doron, K. Yanuka-Golub, T. Olender, R. Hadar, G. Rosenberg, R. Jain, J. Cámara-Almirón, D. Romero, S. van Teeffelen, and I. Kolodkin-Gal, The extracellular matrix protein TasA is a developmental cue that maintains a motile subpopulation within *Bacillus subtilis* biofilms, Sci. Signaling **13**, eaaw8905 (2020).

[25] G. Ravel, M. Bergmann, A. Trubuil, J. Deschamps, R. Briandet, and S. Labarthe, Inferring characteristics of bacterial swimming in biofilm matrix from time-lapse confocal laser scanning microscopy, eLife **11**, e76513 (2022).

[26] J. P. Thiery, Epithelial-mesenchymal transitions in tumour progression, Nat. Rev. Cancer **2**, 442 (2002).

[27] J. Stenhammar, R. Wittkowski, D. Marenduzzo, and M. E. Cates, Activity-induced phase separation and self-assembly in mixtures of active and passive particles, Phys. Rev. Lett. **114**, 018301 (2015).

[28] A. Wysocki, R. G. Winkler, and G. Gompper, Propagating interfaces in mixtures of active and passive brownian particles, New J. Phys. **18**, 123030 (2016).

[29] P. Dolai, A. Simha, and S. Mishra, Phase separation in binary mixtures of active and passive particles, Soft Matter **14**, 6137 (2018).

[30] S. R. McCandlish, A. Baskaran, and M. F. Hagan, Spontaneous segregation of self-propelled particles with different motilities, Soft Matter **8**, 2527 (2012).

[31] S. Saha, J. Agudo-Canalejo, and R. Golestanian, Scalar active mixtures: The nonreciprocal Cahn-Hilliard model, Phys. Rev. X **10**, 041009 (2020).

[32] V. Ouazan-Reboul, J. Agudo-Canalejo, and R. Golestanian, Self-organization of primitive metabolic cycles due to nonreciprocal interactions, Nat. Commun. **14**, 4496 (2023).

[33] A. Dinelli, J. O'Byrne, A. Curatolo, Y. Zhao, P. Sollich, and J. Tailleur, Non-reciprocity across scales in active mixtures, Nat. Commun. **14**, 7035 (2023).

[34] P. Ghosh, J. Mondal, E. Ben-Jacob, and H. Levine, Mechanically-driven phase separation in a growing bacterial colony, Proc. Natl. Acad. Sci. USA **112**, 201504948 (2015).

[35] T. Kolb and D. Klotsa, Active binary mixtures of fast and slow hard spheres, Soft Matter **16**, 1967 (2020).

[36] Q. J. S. Braat, C. Storm, and L. M. C. Janssen, Formation of motile cell clusters in heterogeneous model tumors: The role of cell-cell alignment, Phys. Rev. E **110**, 064401 (2024).

[37] L. Hupe, Y. G. Pollack, J. Isensee, A. Amiri, R. Golestanian, and P. Bittihn, A minimal model of smoothly dividing disk-shaped cells, arXiv:2409.01959.

[38] See Supplemental Material at http://link.aps.org/supplemental/10.1103/9pns-h5ll for details on the numerical model, the clustering analysis, and the fitting procedure for the effective potential, as well as supporting evidence for the coarsening dynamics and bath dynamics near larger objects.

[39] To keep the analysis consistent with subsequent velocity calculations, we take the spatial location to be defined by the corresponding particles' center positions.

[40] J. R. Howse, R. A. L. Jones, A. J. Ryan, T. Gough, R. Vafabakhsh, and R. Golestanian, Self-motile colloidal particles: From directed propulsion to random walk, Phys. Rev. Lett. **99**, 048102 (2007).

[41] C. Bechinger, R. Di Leonardo, H. Löwen, C. Reichhardt, G. Volpe, and G. Volpe, Active particles in complex and crowded environments, Rev. Mod. Phys. **88**, 045006 (2016).

[42] T. Sunkel, L. Hupe, and P. Bittihn, Motility-induced mixing transition in exponentially growing multicellular spheroids, Commun. Phys. **8**, 179 (2025).

[43] S. R. Lish, L. Hupe, R. Golestanian, and P. Bittihn, Isovolumetric dividing active matter, arXiv:2409.20481.

[44] M. Kardar and R. Golestanian, The "friction" of vacuum, and other fluctuation-induced forces, Rev. Mod. Phys. **71**, 1233 (1999).

[45] D. Ray, C. Reichhardt, and C. J. O. Reichhardt, Casimir effect in active matter systems, Phys. Rev. E **90**, 013019 (2014).

[46] J. Bialké, H. Löwen, and T. Speck, Microscopic theory for the phase separation of self-propelled repulsive disks, Europhys. Lett. **103**, 30008 (2013).

[47] B. Waclaw, J. Sopik, W. Janke, and H. Meyer-Ortmanns, Mass condensation in one dimension with pair-factorized steady states, J. Stat. Mech. (2009) P10021.

[48] B. Waclaw and M. R. Evans, Explosive condensation in a mass transport model, Phys. Rev. Lett. **108**, 070601 (2012).

[49] B. Mahault and R. Golestanian, Bose–Einstein-like condensation due to diffusivity edge under periodic confinement, New J. Phys. **22**, 063045 (2020).

[50] J. Bezanson, A. Edelman, S. Karpinski, and V. Shah, Julia: A fresh approach to numerical computing, SIAM Rev. **59**, 65 (2017).

[51] https://inparts.org/.

[52] L. Hupe, J. Isensee, and P. Bittihn, InPartS: Interacting particle simulations in Julia (2022), available at: http://hdl.handle.net/21.11101/0000-0007-FE12-7.

[53] L. Hupe, J. Isensee, and P. Bittihn, InPartSBiome.jl, available at: http://hdl.handle.net/21.11101/0000-0007-FE13-6.

[54] L. Hupe, Example simulation scripts, available at: http://hdl.handle.net/21.11101/0000-0008-007C-D.

[55] S. Danisch and J. Krumbiegel, Makie.jl: Flexible high-performance data visualization for Julia, J. Open Source Software **6**, 3349 (2021).